DOI: 10.1039/b810841b

The good reactivity of lithium with nanostructured copper phosphide

Claire Villevieille,[a] Florent Robert,[a] Pierre Louis Taberna,[b] Laurent Bazin,[b] Patrice Simon[b] and Laure Monconduit*[a]

In Li-ion battery technology, Li diffusion in the electrode is mainly limited by the quality of the interfaces. To take advantage of the large capacity gain offered by the transition metal phosphides (TMP) as negative electrode, a new self-supported TMP/Cu nanoarchitectured electrode concept is proposed. This specific design allows one to fine-tune control of both (TMP)/current collector and (TMP)/electrolyte interfaces of the electrode. This new electrode preparation process is based on an electrochemical templated synthesis of copper nanorods followed by a phosphorus vaporization. The P vapour reacts with the Cu nanorods leading to Cu_3P nanorods. Preliminary electrochemical tests of the as-obtained Cu_3P nanorods/Li half cell show the great interest of using such a nanostructured TMP electrode in a Li battery. These nanoarchitectured phosphide electrodes can sustain a C-rate (a full discharge in 1h) cycling without exhibiting any important reversible capacity loss for 20 cycles.

Introduction

Seeking new materials is a key challenge for the development of Li-ion energy storage systems.[1] Most commercial Li-ion batteries use $LiCoO_2$ (or Co oxide-based materials) as positive electrode and a carbonaceous material as negative electrode. Our work was focused on the negative side of the battery by looking at materials showing greater capacities than graphite while maintaining excellent capacity retention. One of them is the transition metal phosphides (TMP). They are promising negative electrode materials exhibiting high gravimetric and volumetric capacities associated with low electrode volume expansion.[2,3,4] Different redox reactions occur depending on the 3d transition metal. With middle transition metals (M = Mn, Fe, Co, Ni), it generally proceeds through a conversion of MP_y into a composite electrode made of metallic nano-sized particles embedded into a Li_3P matrix ($MP_y + 3yLi \rightarrow yLi_3P + M^0$).[5,6,7] These so-called conversion reactions offer a new type of energy storage process involving more Li exchanged per formula unit than graphite, leading to a higher theoretical capacity. Moreover with Cu-based phosphide compounds, displacement reactions occur.[8] In such reactions, the reversible Cu extrusion–re-injection process leads to an increase of both gravimetric and volumetric capacities (390 $mAh.g^{-1}$, 3020 $mAh.cm^{-3}$) as compared to graphite (350 $mAh.g^{-1}$, 830 $mAh.cm^{-3}$).[9,10] Recently, we succeeded in growing Cu_3P as a thick film over a copper foil by a very simple solid-state reaction at low temperature.[11] Using such a synthesis route, we obtained carbon-free self-supported phosphide electrodes. However, the performances in term of cyclability were not greatly improved. A solution to improve the capacity retention during cycling could be the design of ordered nanostructured electrodes with enhanced specific surface area and shorter Li diffusion lengths to increase the kinetics of reaction. Recently, Simon and co-workers published a two-step electrode design consisting of the electrochemically assisted template growth of Cu nanorods onto a Cu foil current collector followed by electrochemical plating of Fe_3O_4 or Ni_3Sn_4 onto the rods.[12,13] Using such electrodes, they demonstrated a great improvement in power density as well as in capacity retention.

To benefit from the large capacity gain advantages offered by transition metal phosphide based electrodes, we propose here to improve the kinetics of reactions of copper phosphides *vs* Li together with enhancement of their capacity retention by designing new nanoarchitectured electrodes. The process is based on the electrochemical template synthesis of copper nanorods. The as-obtained Cu metallic nano-pillars are then thermally treated under phosphorus vapor. The phosphorus chemically reacts with the copper nanorods leading to Cu_3P/Cu nanorods. We described in this paper a new preparation of copper nanorods by vaporization of the as-prepared pillars by phosphorus. The copper phosphide covered Cu rods were characterized by scanning electron microscopy (SEM)/energy dispersive X-ray (EDX) analysis and X-ray diffraction (XRD). The electrochemical performances of the Cu_3P/Cu nanorods were tested *vs* lithium.

Experimental

Cu nanorods by electrosynthesis

All the deposits were made on a 2 cm^2 large/150μm thick Cu foil from Goodfellow Company (Cu 99.9%) and were mirror polished with sandpaper before use. Copper disks were polished following these successive steps, with 800, 1200 and 2400 grit sand paper and then with 6, 3, 1 and 0.25 micron diamond suspension using a polishing cloth. After this last step, copper disc surfaces exhibited a mirror like look meaning that an object is perfectly reflected without any deformation. The anodized aluminium oxide membranes (AAO) used to make the deposits were 60μm thick (Whatman Company, Anodisc 47-68095022).

[a]*ICG-AIME-UMR 5253—Université Montpellier 2 Place E. Bataillon, Bat. 15, cc15, 34095 Montpellier, Cedex 5, France. E-mail: laure.monconduit@univ-montp2.fr*
[b]*CIRIMAT-UMR 5085—Université Paul Sabatier route de Narbonne, 31062 Toulouse, Cedex 4, France*

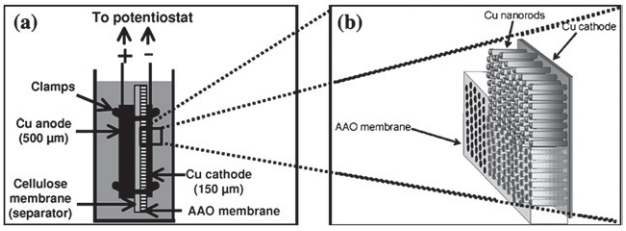

Fig. 1 The electrochemical cell and the nanostructured current collector. a, Diagram of the electrochemical cell used for the template synthesis of the nanostructured Cu current collector. b, Diagram of the nanostructured current collector expected to be obtained at the end of the electrolysis, before and after removal of the AAO membrane.

Copper rod deposition was achieved using a pulsed current method with an Arbin BT2000. A square wave current signal was applied with two currents i_1 (30 mA.cm^{-2}; 50ms) and i_2 (2 mA.cm^{-2}; 250ms). The electrolytic bath was composed of a mixture of $CuSO_4$ (100g/L), $(NH_4)_2SO_4$ (20g/L) and diethyltriamine (80mL/L). All these products were purchased from Acros Organics. The electrolytic cell is described in Fig. 1. The cathode and the anode were stacked together on both sides of the AAO membrane. A cellulosic separator was placed between the anode and the AAO membrane. The assembly was maintained under pressure with the help of stainless steel clamps. Plating time was 1 hour. The substrate was then rinsed in distilled water, and soaked in sodium hydroxide (1mol/L, Acros Organics) to remove the alumina membrane. All the samples as obtained were then stored in an argon filled glove box.

A schematic description of the process is shown in Fig. 1.

P vaporization on Cu nanorods

The second step of the electrode preparation deals with the solid–vapor reaction of the as-prepared Cu nanorods with phosphorus. Cu nanorods were disposed in one compartment of a two-compartment vacuum sealed quartz ampoule with, in the other compartment, stoichiometric amounts of red phosphorus powder. A survey of various temperatures (ranging from 260 °C to 300 °C) and reaction times (0 to 1 hour) was conducted and is summarized in Table 1.

The quartz vessels were placed into an oven and once the selected annealing temperature profile was completed, the oven was turned off, the tube opened and the phosphorus Cu recovered substrate characterized by X-ray analysis and by both SEM and EDX.

The morphology of metallic and TMP rods materials was determined by scanning electron microscopy (SEM, JEOL 1200 EXII). Semi-quantitative energy-dispersive X-ray spectroscopy (EDX) analysis of the nanowires shows the mole ratio of the main elemental components. To explore the core of the nanorods we used the microtome technique. The nanorod samples were embedded in epoxy resin and then cut with an ultramicrotome using a diamond knife. As the epoxy resin infiltrates the space between the rods, the electrode structure is preserved during the sectioning process. It yields sections of rather homogeneous thickness, which allows cross-sectional area to be examined.[14]

Electrochemical tests vs Li

To test the as-prepared TMP electrode *vs* Li, Swagelok-type cells were assembled in an argon filled glove box and cycled using a Mac Pile automatic cycling/data recording system (Biologic Co, Claix, France). The cells were cycled between 2.5V (or 2V) and 0.02V vs Li^+/Li^0 at a cycling rate of C/n (that is one full discharge or charge in n hours). These cells were assembled using a Li metal disc as both negative electrode and reference electrode, a Whatman GF/D borosilicate glass fiber sheet saturated with a 1 M $LiPF_6$ in ethylene carbonate (EC):dimethyl carbonate (DMC) (1:1 in weight) as the electrolyte, and a nanostructured Cu_3P/Cu electrode as positive electrode. It is important to notice that SEM images (not shown) of the nano-pillars after cycling do not show any deformation under the pressure inside the Swagelok.

Results

Structural studies of the Cu nanorods obtained by the electrosynthesis described in the experimental section and in Fig. 1

Table 1 Thermal treatments conditions for the P vaporization and resulting Cu/P ratio deduced from the EDX analysis. "Water quenching" means that the silica tube is plunged into water (at 10 °C) after the thermal treatment

	Annealing treatment					
Number of tests	T/°C	Duration	Thermal rate (up)	Thermal rate (down)	Averaged atomic % Cu/P (EDX)	Morphology
1	350	0 min	0.1 °C/min	Water quenching	76/24	destroyed
1	350	0 min	0.1 °C/min	10 °C/min	75/25	destroyed
1	330	0 min	0.1 °C/min	Water quenching	77/23	destroyed
2	300	0 min	0.2 °C/min	10 °C/min	77/23 (75/25)	destroyed
1	300	0 min	1 °C/min	Water quenching	72/28	destroyed
2 (Fig. 3B)	300	0 min	0.1 °C/min	Water quenching	75/25 (72/28)	destroyed
1	300	0 min	0.2 °C/min	Water quenching	75/25	nano-structured
1	290	0 min	0.2 °C/min	Water quenching	×	nano-structured
1	290	0 min	1 °C/min	Water quenching	77/23	partially aggregated
1	290	0 min	0.1 °C/min	Water quenching	77/24	nano-structured
2 (Fig. 3D)	290	0 min	0.1 °C/min	Water quenching	75/25 (72/28)	nano-structured
1	280	0 min	0.1 °C/min	Water quenching	94/6	nano-structured
1	270	30min	0.1 °C/min	Water quenching	76/24	nano-structured
1 (Fig. 3C)	270	1h	0.1 °C/min	Water quenching	78/22	nano-structured
1 (Fig. 3A)	260	1h	0.1 °C/min	Water quenching	95/5	nano-structured

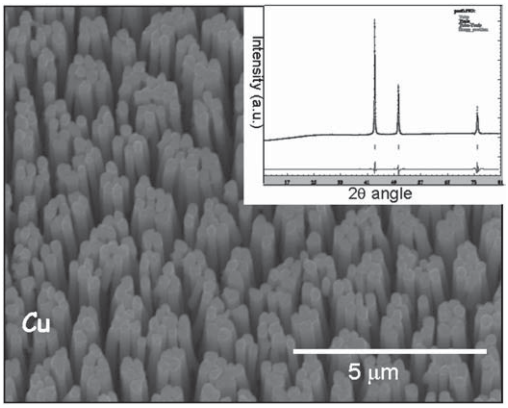

Fig. 2 SEM image and X-ray diffraction pattern ($CuK\alpha_1$) of the copper nanopillars and its refinement obtained by full pattern matching using Winplotr Software.

were carried out by X-ray diffraction and scanning electron microscopy.

Fig. 2 shows top views of the Cu nanorod current collector after AAO membrane removal. The Cu foil is covered with distributed copper rods of about 200 nm in diameter as defined by the alumina membrane pore size, and a height of 7 μm. Copper (Fm3m, a = 3.6077Å) is identified by X-ray diffraction (Fig. 2, inset).

Table 1 summarizes the thermal conditions used for the phosphorus vaporization on the Cu nanopillars. Various thermal treatments were performed to combine the expected 75/25 atomic% in Cu/P with the nanostructuration of the electrode.

The treatment temperature was initially chosen around 277 °C which is the phosphorus boiling temperature. Table 1 shows that the thermal treatments with temperatures higher than 300 °C lead to the destruction of the Cu nanostructure, as illustrated by the nice crystallized flat Cu_3P surface in Fig. 3B. In contrast, we found that lowering the temperature below 270 °C leads to a partially phosphorus surface, and no CuP_x phases were obtained, independently of the reacting time (Fig. 3A). Thus, we tested the annealing treatments between 300 and 270 °C with varying reacting times from 0 to 1 hour. In these conditions we systematically obtained the expected 3Cu/1P molar ratio by EDX analyses as indicated in the insets of Fig. 3B–D.

When water quenching was done, the nanostructuration was retained (Fig. 3C,D), while a lower cooling rate (10 °C/min) to return to ambient temperature led to the destruction of the rods and gave a highly crystallized Cu_3P surface. It is noteworthy that a flash temperature ($270 < T \leq 300$ °C) treatment allows one to concomitantly achieve electrode nanostructuration as well as deposition of the Cu/P expected composition. The slight excess of Cu revealed by the EDX analyses could be due to a contribution from the copper of the substrate. A 300 °C thermal treatment with a larger amount of phosphorus leads to the formation of a CuP_2 phase. SEM images show that a P thermal treatment with $260<T<300$ °C does not strongly modify the size of the rods.

To explore the nature of the core of the phosphorus copper nanorods (Cu or Cu_3P), we used SEM on the cross-sectional areas of the rods (see experimental section). The Z-contrast back scattered electrons (BSE) are expected to differentiate the native Cu with a white contrast from the Cu_3P with a darker contrast. The core of the phosphorus samples appears white (Fig. 4B) like the nanorods before phosphorus thermal treatment (Fig. 4A), while the external layer around each rod shows the expected gray contrast for Cu_3P. We concluded that only the surface of the copper rods reacted with phosphorus to give Cu_3P. The width of the phosphide layer can be evaluated to 20–50 nm.

The crystal structure and phase composition of the treated rods (flash 290 °C treatment followed by a water quenching) were obtained by X-ray diffraction (XRD) (Fig. 5). With the exception of the reflections owing to metallic copper of the substrate, the XRD pattern of the treated rods reveals Bragg peaks which can all be indexed on the basis of a hexagonal cell with the following refined lattice parameters: a = 6.968(1) Å, c = 7.137(2) Å, *P63cm* space group (ICDD 71-2261).[15] Note that Cu_2O is found as a side product.

All the nanostructured phosphorus electrodes were electrochemically tested in Li-half cells. In Fig. 6, the shape of the galvanostatic plot and the associated derivative curve of the Cu_3P/Cu-based electrode appear to be quite identical to those obtained from the Cu_3P-HT powder sample prepared by the classical ceramic route (HT) excepted at low potential where the Cu_3P rods curve displays a smoother shape.[16] On cycling, the common curve profile is maintained. By combining the

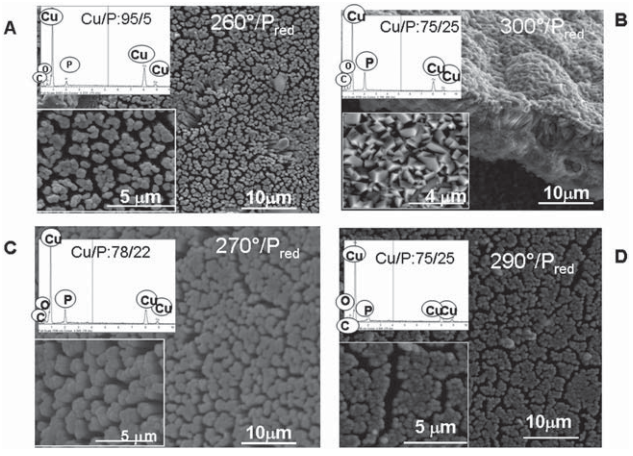

Fig. 3 SEM images and associated EDX results of Cu nanopillars A) after 260 °C/1h phosphorus heat treatment, B) after 300 °C/0h phosphorus heat treatment, C) after 270 °C/1h phosphorus heat treatment and D) after 290 °C/0h phosphorus heat treatment.

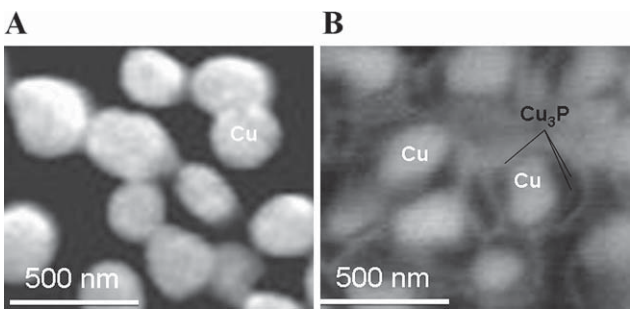

Fig. 4 SEM images of the cross-sectional area of A) the pristine Cu nanorods and B) treated Cu_3P/Cu nanorods after embedding in epoxy resin and cutting with an ultramicrotome using a diamond knife.

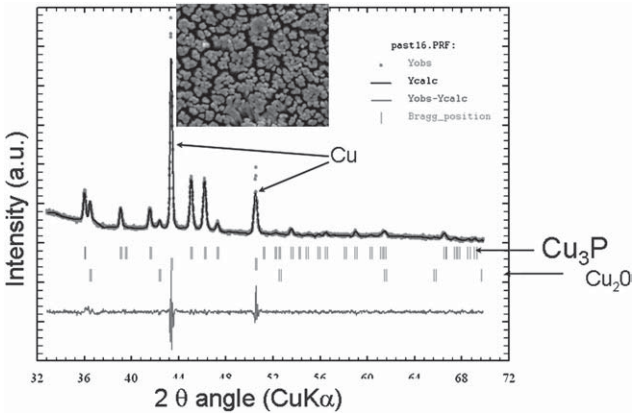

Fig. 5 X-Ray diffraction pattern ($CuK\alpha_1$) of copper nanopillars after 290 °C/0h phosphorus heat treatment and its refinement obtained by full pattern matching using Winplotr Software.

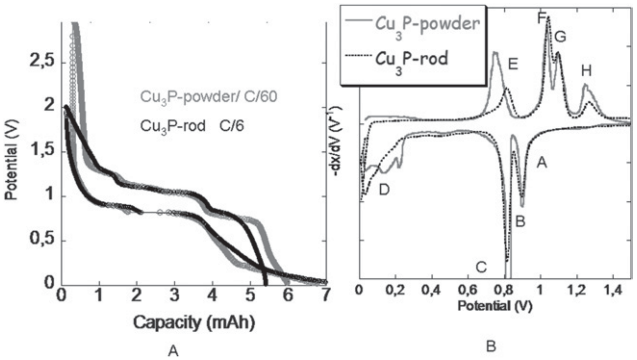

Fig. 6 A) Voltage–composition curve for a Li half-cell, using a Cu_3P/Cu nanorod as the positive electrodes (black line), and cycled between 2.0 to 0.1V. The HT-Cu_3P powder galvanostatic curve (grey line) is given for comparison. B) The associated derivative curves to identify the successive electrochemical processes.

electrochemical analysis and the associated in *situ* XRD results, the electrochemical mechanism for the Cu_3P-HT sample *vs* Li was previously identified.[17] The discharge proceeds by lithium insertion into the Cu_3P hexagonal structure (A process) and then by two successive bi-phasing processes involving the formation of $LiCu_2P$ (B process) and Li_2CuP (C process). Simultaneously, copper metal is extruded from the matrix. If completely reduced a last step occurs (D) which is $Li_2CuP + Li \rightarrow Li_3P + Cu^0$. All these steps are fully reversible on charge, through the E, F, G and H processes. The full cycle of the Cu_3P powder/Li battery led to 350 $mAh.g^{-1}$. However, the first cycle irreversibility of the Cu_3P powder sample was high and after 10 cycles more than 50% of the capacity has been lost, indicative of a decrease in the reversibility of the reaction due to both kinetic limitations and materials degradation on cycling. Our previous study also showed that scan rate affects the electrochemical performances of Cu_3P powder anodes: the slower the scan rate, the higher the initial capacity. Moreover, it was pointed out that nanosized Cu_3P powders favored high initial capacity values and that the scan rate was then more effective on crystallized powder rather than on amorphous powder. In contrast, it appeared that the microsized Cu_3P powder showed better capacity retention than the nanosized powder.

The present nanostructured Cu_3P samples were electrochemically tested versus Li, at various cycling rates. For comparison, similar measurements were performed on a Li half cell using a Cu_3P film obtained at 300 °C (Fig. 3B) for which the nanostructure was fully destroyed. Impressive 0.6 to 2 $mAh.cm^{-2}$ normalized Q capacities (towards the geometrical surface area) were measured at different scan rates. The variation of the normalized Q capacity as a function of the applied rate expressed in terms of C/n (C/n being defined as the full discharge in n hours) is shown in Fig. 7. As previously observed for the powder, we observe that the scan rate strongly affects the capacity values, with a capacity measured at C/60 rate three times higher than that measured at C rate. However, for all the measurements recorded at C, C/20 and C/60 rates, the capacity to store lithium is maintained at high values for the nanostructured samples with no sign of any significant decay, compared with the Cu_3P thick films cells, and "a fortiori" with the powder samples. No loss of capacity is observed during the 40 first cycles. By contrast the capacity of the Cu_3P thick film-based electrode rapidly fades. The scanning electron microscopy observation of a Cu_3P thick film-based electrode after 40 cycles showed cracks on the film electrode surface (inset Fig. 7), thus limiting its life-time. The nanorods offer free space to accommodate their expansion during lithium uptake and demonstrate the benefit of the nanostructuration.

Whatever the rate used, an irreversible capacity is observed in all the experiments during the first cycle. This irreversibility can be explained i) by the presence of Cu_2O (see Fig. 5) and ii) by the electrolyte reaction increased by the higher surface area electrode/electrolyte.

The chemical growth of Cu_3P layers from the Cu of the rods is expected to be more advantageous than a simple coating. It alloys to maintain a high capacity at high rate. The performance improvement of this new self-supported phosphide electrode is linked to i) an ideal chemical interface between Cu_3P active

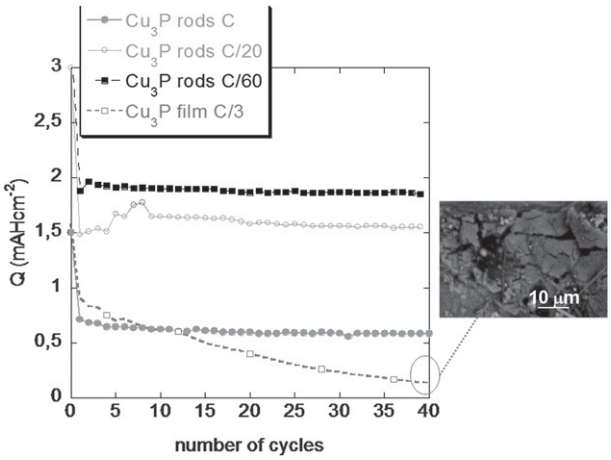

Fig. 7 The capacity retention of the Cu_3P/Cu nanorod based half cells cycled at C (gray circles), at C/20 (open gray circles) and at C/60 (black squares) rates, between 2.5 to 0.1V. The capacity retention of a Cu_3P thick film (open squares) is given for comparison. In inset, a SEM image of the surface of the Cu_3P thick film after cycling.

material and copper current collectors in the core of each rod (the electronic transport is optimized), ii) a high interface surface area between the active material and the liquid electrolyte (the ionic transport is optimized) and iii) a buffering of the volume variations upon cycling by the free volume between the rods. The enhancement of the interface contacts aims at countering kinetic limitations of phosphide active materials.

These self-supported electrodes of Cu_3P produce a significant improvement of the electrochemical performances previously obtained with Cu_3P powder, especially with regard to the rate capability and the retention efficiency (two of the well-known limitations of transition metal phosphide electrodes). Using such a configuration, we obtained carbon-free self-supported Cu_3P electrodes capable of sustaining higher capacities over many cycles while having enhanced rate capabilities. These new self-supported Cu_3P/Cu electrodes, based on chemically made interfaces, offer new opportunities to fully exploit the capacity gains provided by phosphide materials. Needless to say, the use of such nanostructured electrodes is mainly interesting for special microdevices or fundamental work.

Acknowledgements

This research was performed in the framework of Advanced Lithium Energy Storage Systems Network of Excellence (contract N° SES6-CT-2003-503532) founded by the European Commission). The authors are grateful to Dr Y. Nedellec (ICG-AIME, France) for microtome cut and SEM measurements.

References

1 P. Bruce, Bruno Scrosati and Jean-Marie Tarascon, *Angewandte Chemie, International Edition*, 2008, **47**(16), 2930–2946.
2 M. L. Doublet, F. Lemoigno, F. Gillot and L. Monconduit, *Chem. Mat.*, 2002, **14**(10), 4126.
3 D. C. S. Souza, V. Pralong, A. J. Jacobson and L. F. Nazar, *Science*, 2002, **296**(5575), 2012–5.
4 M. V. V. M. Satya Kishore and U. V. Varadaraju, *Pow Sources*, 2006, **156**(2), 594–597.
5 S. Boyanov, J. Bernardi, F. Gillot, L. Dupont, M. Womes, J.-M. Tarascon, L. Monconduit and M. L. Doublet, *Chem. Mat*, 2006, **18**, 3531.
6 F. Gillot, S. Boyanov, L. Dupont, M.-L. Doublet, M. Morcrette, L. Monconduit and J.-M. Tarascon, *Chem. Mat*, 2005, **17**, 6327.
7 O. Crosnier and L. F. Nazar, *Electrochem Sol-State Lett*, 2004, **7**(7), A187–A189.
8 V. Bodenez, L. Dupont, M. Morcrette, C. Surcin, D. W. Murphy and J.-M. Tarascon, *Chem. Mater.*, 2006, **18**(18), 4278–4287.
9 K. Wang, J. Yang, J. Xie, B. Wang and Z. Wen, *Electrochem. Comm*, 2003, **5**, 480.
10 M. P. Bichat, T. Politova, J. L. Pascal, F. Favier and L. Monconduit, *J. Electrochem. Soc*, 2004, **12**, A2074.
11 H. Pfeiffer, F. Tancret, M. P. Bichat, L. Monconduit, F. Favier and T. Brousse, *Electrochem. Comm*, 2004, **6**, 263.
12 P.-L. Taberna, S. Mitra, P. Poizot, P. Simon and J.-M. Tarascon, *Nature Materials*, 2006.
13 J. Hassoun, S. Panero, P. Simon, P. L. Taberna and B. Scrosati, *Adv. Mat*, 2007, **19**, 1635.
14 D. A. Blom, J. R. Dunlap, T. A. Nolan and L. F. Allard, *J. Electrochem. Soc*, 2003, **150**, A414.
15 O. Olofsson, *Acta Chem. Scand*, 1972, **26**, 2777.
16 M. P. Bichat, T. Politova, H. Pfeiffer, F. Tancret, L. Monconduit, J. L. Pascal, T. Brousse and F. Favier, *Pow. Sources*, 2004, **136**, 80–87.
17 B. Mauvernay, M.-L. Doublet and L. Monconduit, *J. Physics Chem. Sol*, 2006, **67**, 1252.